SUPPLEMENTARY MATERIAL

A new molecular interpretation of the toughness of multiple network elastomers at high temperature

Juliette Slootman, C. Joshua Yeh, Pierre Millereau, Jean Comtet* and Costantino Creton*

Laboratoire SIMM, ESPCI Paris, PSL University, CNRS, Sorbonne Université, 10 Rue Vauquelin, 75231 Paris Cédex 05

*jean.comtet@espci.psl.eu
*costantino.creton@espci.psl.eu

SI.1. Material synthesis

Most of the materials presented in the paper were synthetized using bulk (solvent-free) monomers, with synthesis as described below.

Another family of Ethyl Acrylate networks was synthetized in the presence of various amounts of solvent in order to continuously vary the prestretch. Synthesis of that series of samples was previously described by Millereau et al. [1] and network properties are recalled in SI.4.

Reactants.

The monomer ethyl acrylate (EA) or methyl acrylate (MA) and the crosslinker butanediol bis(acrylate) (BDA) were purified over a column of activated alumina to remove the inhibitor. The UV initiator, 2-hydroxy-2- methylpropiophenone (HMP) was used as received. All reagents were purchased from Sigma Aldrich. The synthesis of the networks was carried out in a glove box (Mbraun Unilab) under a nitrogen atmosphere to avoid side reactions with the oxygen of the air. Before the introduction in the glove box, every reagent and solvent was bubbled with nitrogen for 45 minutes to remove the dissolved oxygen.

Filler network synthesis.

Samples were prepared through a free radical photo polymerization. 2 hydroxy 2 methylpropiophenone (HMP) was used as a UV initiator. The standard cross linker used was 1,4-butanediol diacrylate (BDA). Monomer, cross linker and initiator (1.16 mol% relative to monomer) were mixed together and the liquid solution was cast in a mold. The latter was composed of two glass plates covered with transparent PET films (with a hydrophobic surface), with a silicone spacer to control the sample thickness (0.7 mm) and two metal frames to seal the mold. The mold was placed under UV for two hours (UV light was produced by a Vilbert Lourmat lamp, model VL-215.L, focused on 365 nm). The UV power was kept low (10 µW/cm2) to create a slow polymerization, the goal being to decrease the number of simultaneously growing chains and the number of termination reactions.

After polymerization, the sample was dried overnight under vacuum (without heating) to remove unreacted volatile monomer. The sample was weighed before and after drying. The weight loss was less than 0.2 %.
The cross-linker concentration was adjusted to tune the properties of the various materials (see Table S1). For each material, up to 3 samples were obtained from distinct polymerization. For each polymerization, run on the same day, the reactive medium was taken from the same pot (monomer, crosslinkers), the initiator was added prior to each polymerization.

Incorporation of mechanophore in the filler network.

In order to label the filler network with mechano-fluorescent molecules, the Diels-Alder adduct mechanophore (DACL) was covalently incorporated as a cross-linker (see [2] for details on the DACL synthesis). DACL was used in combination with the standard crosslinker, BDA. The mechanophore cross-linker was introduced at the 0.02 mol% relative to monomer. This small quantity was enough for damage detection by fluorescence (see SI.4. for discussion on damage quantification).

	HMP (mol%)	Total Cross-linker (mol%)	BDA (mol%)	DACL (mol%)
PMA-DA-0.4	1.16	0.43	0.41	0.02
PEA-DA-0.5	1.16	0.5	0.48	0.02

Table S1. Composition of the various materials. mol% is with respect to monomer concentration. These materials are similar to the one described in [2].

The mechano-fluorescent networks were used as mechano-fluorescent filler networks in multiple networks, with swelling/polymerization steps as described below.

Preparation of multiple network elastomers

The preparation of multiple network elastomers was carried out through multiple steps of polymerization. A piece of filler network, with or without mechanophore, of dimension 20 mm x 40 mm was cut. The cut sample was put in a bath containing the monomer ethyl or methyl acrylate (45 mL), cross-linker (0.01 mol%) and initiator (0.01 mol%). The sample was swollen up to equilibrium for 2 h. The swollen sample was then extracted from the swelling bath and put between two glass slides for UV polymerization of the matrix network within the filler network. The sample was dried overnight under vacuum (without heating).

Multiple networks can be described by the fraction ϕ_{SN} of filler network within the final material and equivalently by the degree of prestretching $\lambda_0 = (\phi_{SN})^{-1/3}$ of the filler network. ϕ_{SN} and λ_0 are calculated from the weight of the filler network and of the final material respectively $\mathrm{m_{SN}}$ and m_{total}, as:

$$\phi_{\mathrm{SN}} = \frac{m_{\mathrm{SN}}}{m_{\mathrm{total}}} \text{ and } \lambda_0 = (\phi_{SN})^{-1/3} = \left(\frac{m_{\mathrm{total}}}{m_{\mathrm{SN}}}\right)^{1/3}$$

To get a higher degree of prestretching of the filler network, λ_0, swelling/polymerization steps were repeated. A higher prestretching of the filler network leads to a higher level of dilution of this filler network in the matrix.

Name	Type of MN	Filler monomer	Matrix monomer	ϕ_{SN}	λ_0	[DACL] (mol/m^3)
SN.EA	SN	EA	-	1	1	2.2

SN.MA	SN	MA	-	1	1	2.8
DN.EA.EA	DN	EA	EA	0.2	1.6	0
DA.DN.EA.EA	DN	EA	EA	0.2	1.6	0.5
DA.DN.MA.EA	DN	MA	EA	0.3	1.5	0.9
DN.MA.MA	DN	MA	MA	0.3	1.6	0
DA.DN.MA.MA	DN	MA	MA	0.3	1.6	0.7
TN.EA.EA	TN	EA	EA	0.07	2.4	0
DA.TN.EA.EA	TN	EA	EA	0.07	2.3	0.2
TN.MA.MA	TN	MA	MA	0.08	2.3	0
DA.TN.MA.MA	TN	MA	MA	0.08	2.3	0.2

Table S2. Summary of the various materials. DACL is incorporated in the first network. DA stands for Diels Alder and characterizes networks containing mechanophores. SN, DN and TN stand respectively for Single, Double and Triple networks. The last letters (EA or MA) characterize the nature of the polymer used respectively in the filler network and in the matrix.

SI.2. Mechanical measurements

Experimental set-up. Crack propagation tests were performed on standard tensile Instron machines, model 5565 or 5965. Samples of dimensions 5 mm x 25 mm were cut out of 0.5 mm to 1.9 thick sheets. A 1 mm notch was introduced by using always a new very sharp razor blade, to obtain as little bulk damage as possible. Two white marks were drawn 5 mm from the notch to follow the stretch locally. The sample was fixed using pneumatic clamps. During the test, an extensometer tracked and recorded the distance between these two marks on the sample on either side of the crack. Force and nominal deformation were measured until failure of the sample. The temperature was controlled from -5°C to 80°C by an oven connected to liquid nitrogen. The crosshead velocity was varied between 5 and 500 µm.s^{-1}, leading to stretch rates between 3.10^{-4} and 3.10^{-2} s^{-1}. At the end of the crack propagation test, broken samples were collected and kept in the fridge before further post-mortem confocal analysis.

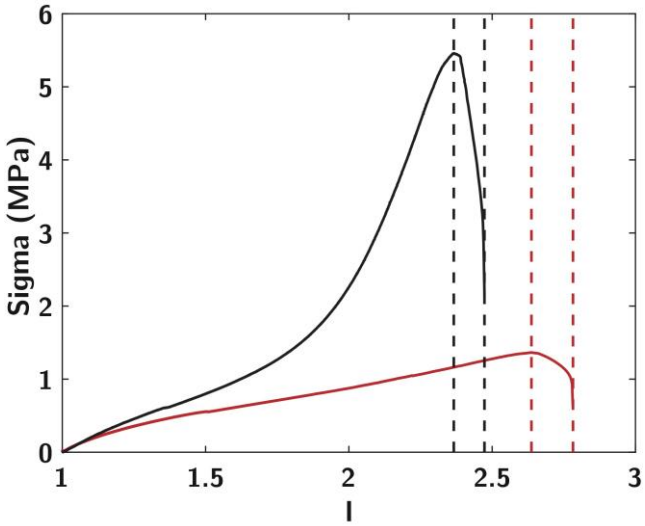

Figure S1. Measurement of fracture energy and crack propagation speed from stress-strain curves. The maximum in stress-strain curve at $\lambda = \lambda_c$ is taken as the point of crack initiation (first vertical dashed line). Crack propagation time is taken as the time from crack initiation to sample failure (second vertical dashed lines). This stress-strain curve corresponds to respectively DA.DN.MA.MA and DA.TN.MA.MA fractured at 25 °C and $\dot{\lambda} = 3 \cdot 10^{-3}$ s^{-1}.

Fracture energy. Following Greensmith, [4] we estimate the fracture energy Γ_c from experiments made on a single edge notch geometry with a crack length smaller than the sample thickness. The fracture energy is approximated as:

$$\Gamma_c = \frac{6\,W(\lambda_c)a}{\sqrt{\lambda_c}}$$

where a is the crack length, λ_c the critical extension at which the crack starts to propagate, and $W(\lambda)$ the strain energy per unit volume. $W(\lambda_c)$ is classically obtained by calculating the area under the curve up to λ_c of the stress-strain curve of an un-notched sample. In our case, to conserve material and optimize experimental efficiency, the fracture energies were estimated directly from the notched stress strain curve (Fig. S1). This measurement leads to a slight under estimations of the fracture toughness for all conditions but allows for quantitative relative comparisons between samples. One to three samples were tested for each experimental condition.

Crack propagation speed. The maximum of the stress strain curves was identified as the time of crack initiation and used for the estimation of the crack propagation time t_{crack} until sample failure (Fig. S1). The crack speed v_{crack} was estimated as $v_{crack} = d_{crack}/t_{crack}$ with $d_{crack} \approx$ 4 mm the crack propagation length.

Mechanophore incorporation does not affect mechanical properties.

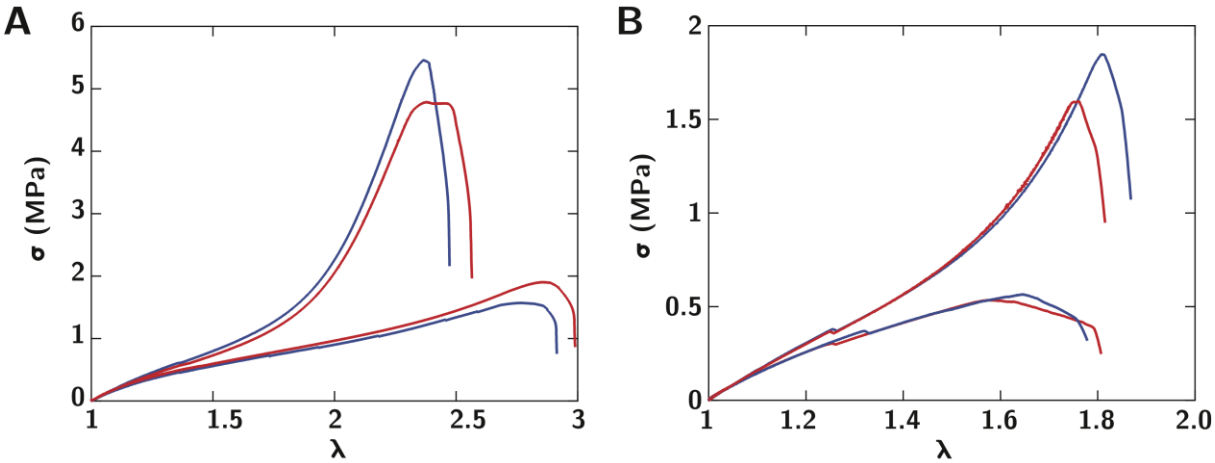

Figure S2. Stress-strain curves of notched double and triple network samples made of **(A)** EA and **(B)** MA networks. With mechanophore (in blue) and without mechanophore (in red) at room temperature.

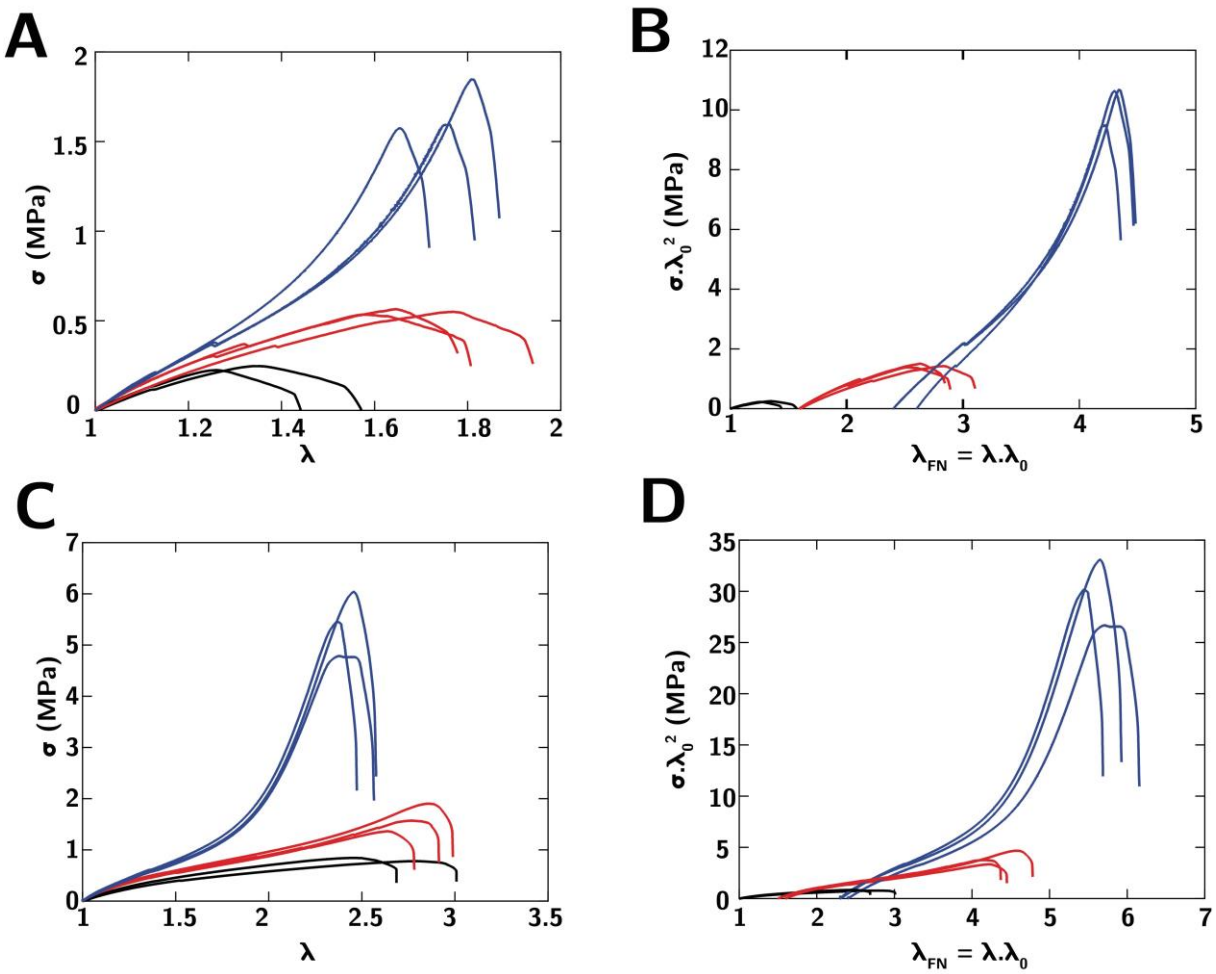

Figure S3. Stress-strain curves of notched samples of **(A-B)** EA and **(C-D)** MA. Black, red and blue correspond respectively to single, double and triple network. In (B) and (D) we observe an increase in the effective filler network stretch at break $\lambda_c\lambda_0$.

SI.3. Network properties and characterization

Areal chain density of filler network in multiple networks

As described previously [2], the cross-link density ν_x^{SN} in the filler network is measured based on the stress-strain curves of the as-synthetized single network.

From gaussian statistics, we can express $\Sigma_{\mathrm{LT}}^{\mathrm{SN}}$, the areal density of polymer strand crossing an arbitrary plane in the Single Network material, as:

$$\Sigma_{\mathrm{LT}}^{\mathrm{SN}} = 1/2 \cdot \nu_x \langle R_0^2 \rangle^{1/2} = \frac{l_0 E_{\mathrm{x}} \sqrt{C_\infty N_x}}{6 k_{\mathrm{B}} T} = l_0 \left(\frac{E_{\mathrm{x}} \rho N_{\mathrm{A}} C_\infty}{6 M_0 k_{\mathrm{B}} T} \right)^{1/2}$$

with ν_{x} the bulk density of elastic chains, $\langle R_0^2 \rangle^{1/2}$ the average distance between crosslinks, l_0 the length of a C-C bond, E_{x} the modulus due to crosslinking, ρ the density of the monomer, and M_0 the molar mass of the monomer, T the temperature, and k_{B} the Boltzman constant. The parameters used for EA and MA network are reported below:

	l_0 (nm)	C_∞	ρ (kg.m^{-3})	M_0 (g.mol^{-1})
MA	0.154	8.1	1220	86.09
EA	0.154	9.3	1120	100.12

Table S3. Parameters used for the estimation of areal chain density. Values of C_∞ and ρ from [5].

In the case of Multiple Networks (MN), the cross-link density and the areal density of chain of the filler network is diluted in the matrix and is given by

$$\nu_{\mathrm{x}}^{\mathrm{MN}} = \frac{1}{\lambda_0^3} \nu_{\mathrm{x}}^{\mathrm{SN}} \text{ and } \Sigma_{\mathrm{LT}}^{\mathrm{MN}} = \frac{1}{\lambda_0^2} \Sigma_{\mathrm{LT}}^{\mathrm{SN}}$$

With ν_x^{SN} and $\Sigma_{\mathrm{LT}}^{SN}$ the cross-link density and areal density of the filler network (Single Network) alone.

Estimation of parameters for multiple networks

	E	T_{g}	ν_x	Σ_{LT}	λ_0
SN.MA	1.15 MPa	18 °C	4.6 10^{25} m^{-3}	1.9 10^{17} m^{-2}	1
SN.EA	1 MPa	-18 °C	4.2 10^{25} m^{-3}	1.8 10^{17} m^{-2}	1
DN.MA.MA	1.9 MPa	18 °C	1.1 10^{25} m^{-3}	7.7 10^{16} m^{-2}	1.6
DN.EA.EA	1.3 MPa	-18 °C	1 10^{25} m^{-3}	6.7 10^{16} m^{-2}	1.6
DN.MA.EA	1.2 MPa	-8 °C	1.4 10^{25} m^{-3}	8.9 10^{16} m^{-2}	1.5
TN.MA.MA	2.2 MPa	18 °C	3.8 10^{24} m^{-3}	3.6 10^{16} m^{-2}	2.3
TN.EA.EA	1.7 MPa	-18 °C	3.5 10^{24} m^{-3}	3.1 10^{16} m^{-2}	2.3

Table S4. Parameters of multiple networks. Modulus E at 25°C, Glass transition temperature T_g, Cross-link density ν_{x} of the filler network, C-C bonds per strand N_x, Strand areal density Σ_{LT} and prestretch λ_0. The glass transition temperature T_{g} of the networks is measured from Dynamic Mechanical Analysis, based on estimation of the inflexion point of the storage modulus. For PMA networks, we have $N_x = 370$ and for PEA networks, $N_x = 320$.

Limiting chain extensibility

To characterize the non-linear behavior of the material, it is instructive to compare the effective stretch of the first network to the limiting extensibility λ_{limit} of the chains of the filler network, defined as:

$$\lambda_{\text{limit}} = \sin\left(\frac{\theta}{2}\right)\left(\frac{6\rho RT}{C_\infty M_0 E_{\text{x}}}\right)^{\frac{1}{2}} = \sin\left(\frac{\theta}{2}\right)\sqrt{\frac{N_x}{C_\infty}}$$

where $\theta = 70.5\ °$ is the complement of the valence angle of the C-C bond, ρ is the density of the polymer, C_∞ is its structure factor, M_0 is the molecular weight of the monomer, E_{x} is the modulus of the filler network due to crosslinks and N_x is the number of C-C bonds per strand. We have respectively $E_{\text{x}}(\text{EA}) = 0.5$ MPa and $E_{\text{x}}(\text{MA}) = 0.6$ MPa (see Slootman et al. [2]), giving $\lambda_{\text{limit}}(\text{EA}) = 4.8$ and $\lambda_{\text{limit}}(\text{MA}) = 5.5$. To compare both networks in the main text, we take the average value $\lambda_{\text{limit}} = 5.1$.

Linear viscoelasticity, time temperature superposition, and shift factor

The temperature and frequency dependence of the samples were tested with a RDAII parallel plate rheometer (Anton Paar, Physica MCR 501). The samples were cut in disk shape using an 8 mm diameter puncher. To avoid slippage from the geometry, samples were glued using Loctite 406. The limits of the linear regime were first determined for all samples, at three different temperatures. A deformation sweep was applied at 1 Hz from 0.01 % to 1 % at 20 °C and 40 °C and from 0.01 % to 0.4 % at -10 °C.
A frequency sweep was then applied from 0.063 to 63 rad.s-1 every 1.5 °C between - 10 °C and 80 °C. The strain was fixed at 0.02 % to be in the linear regime. Using the time temperature superposition principle, data taken at different temperatures were manually shifted to construct a master curve at a reference temperature of 22 °C. The tan δ data obtained for each temperature were first horizontally shifted one by one by a factor a_T until the best fit was achieved. To improve the quality of superposition of the master curve, a vertical shift of b_T was also applied taking into account the temperature and density dependence of the entropic modulus.

$$b_T = \frac{\rho T}{\rho_{\text{ref}} T_{\text{ref}}}$$

where ρ and ρ_{ref} are the density at T and T_{ref} respectively.

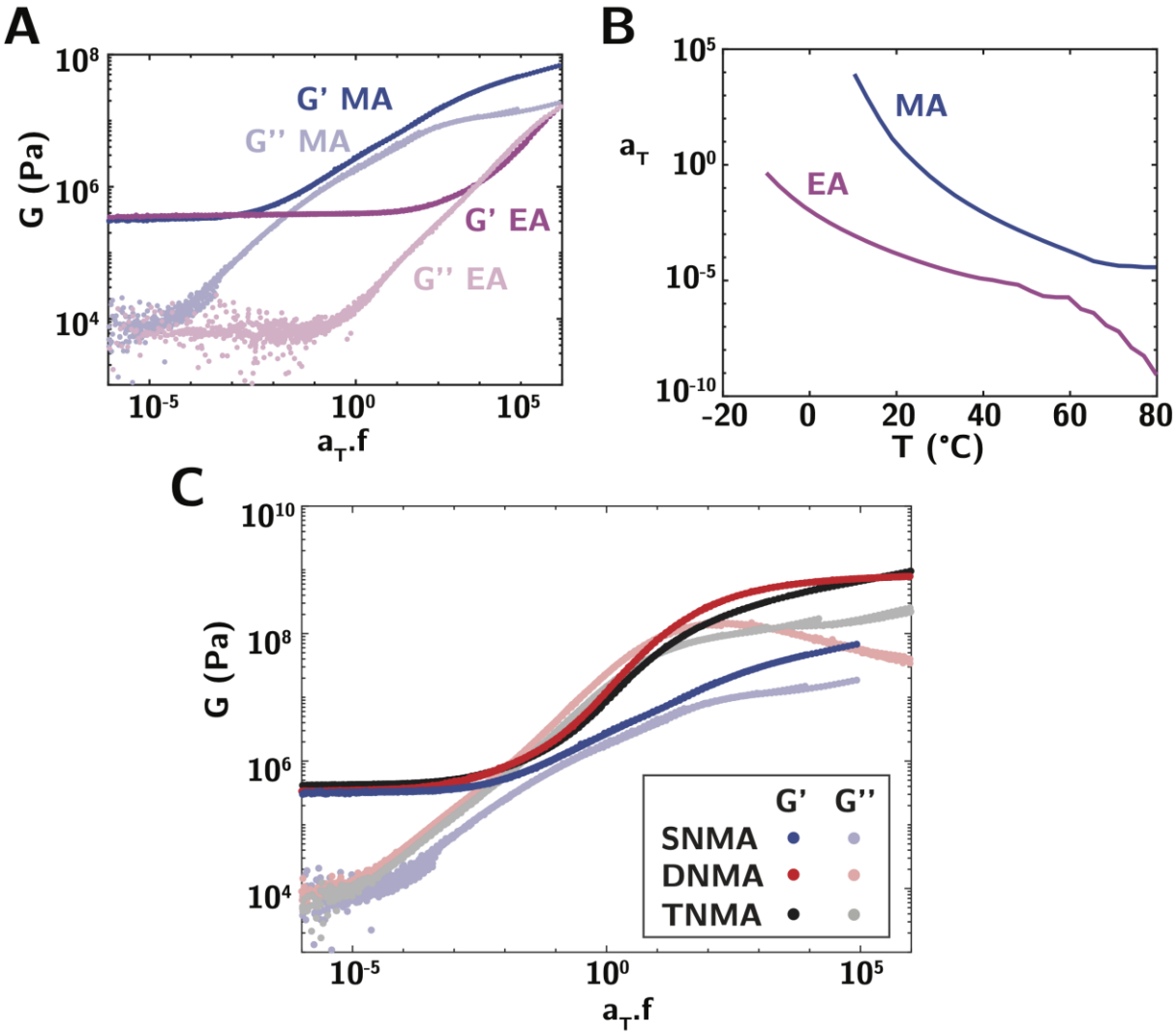

Fig. S4. Linear viscoelasticity, time temperature superposition, and shift factor (A) Master curve at T = 25 °C for PMA and PEA single networks. **(B)** Shift factor a_T as a function of ambient temperature, for both PEA and PMA single networks. **(C)** Master curve at T = 25 °C for SN.MA, DN.MA and TN.MA network. The master curves are reconstructed based on frequency sweeps between 0.63 to 63 rad·s^{-1} every 1.5 °C between -10 °C and 80 °C.

SI.4. Second Family of networks synthetized in solvent

Fig. 7 and Figs. S6 show values of the fracture energy for a second class of PEA based networks synthetized in the presence of solvent, and for which the prestretch could be varied continuously. The synthesis was described by Millereau et al. [1]. Materials properties in uniaxial extension are reported in [1]. Note that the presence of solvent during synthesis leads to a less efficient crosslinking and to a decrease of the density of entanglements in comparison with the synthesis in the bulk described in SI.1.

In this family of networks, the cross-linking contribution of the filler network is 0.76 MPa, close to the value of 0.7 and 0.6 MPa for PEA and PMA materials [2].

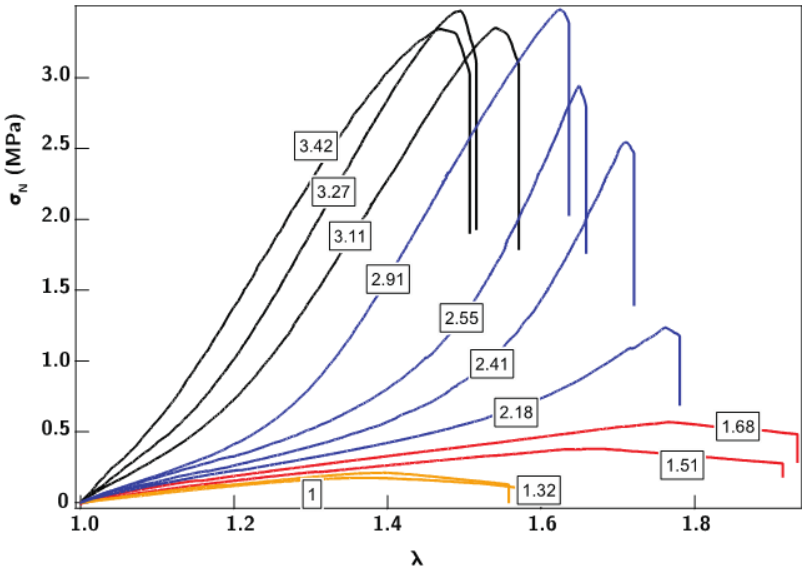

Fig. S5. Stress-strain curves of notched solvent synthetized PEA samples. Stretch rate is $\dot{\lambda} = 2.10^{-2}$ s^{-1} and temperature is $T = 25$ °C. The numbers on each of the curves correspond to the value of the prestretch λ_0.

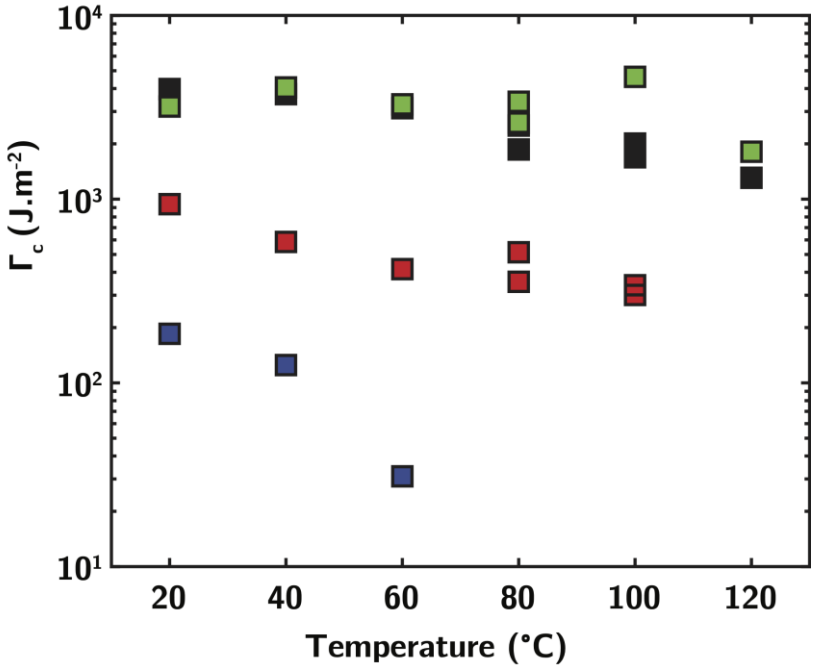

Fig. S6. Variation of the fracture energy Γ_c with temperature (for solvent synthetized PEA samples). Blue symbols (λ_0 = 1), Red symbols (λ_0 = 1.68), Black symbols (λ_0 = 2.55), Green symbols (λ_0 = 3.42). Experiments carried out on notched samples at $\dot{\lambda} = 4.10^{-3}$.

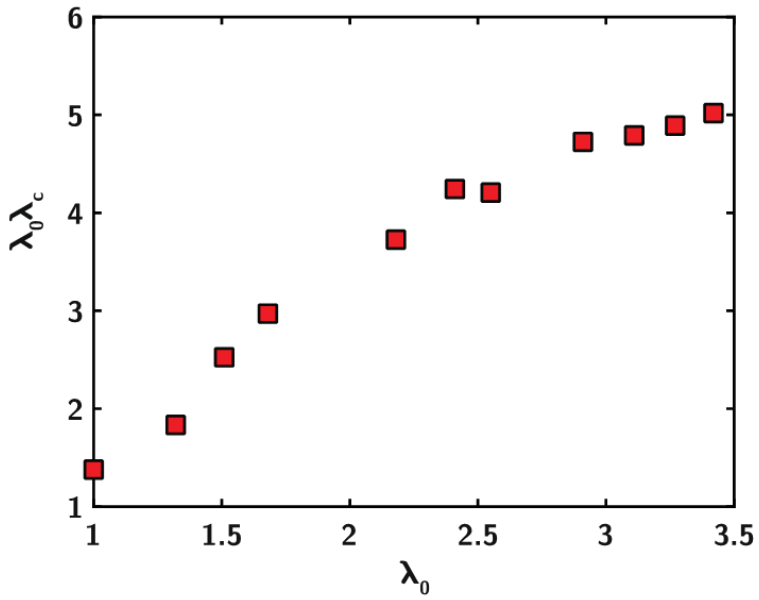

Fig. S7. Variation of the effective critical stretch at break $\lambda_c\lambda_0$ as a function of the filler network prestretch λ_0 (for solvent synthetized PEA samples). Test carried out at $\dot{\lambda} = 4.10^{-3}$ at T = 25°C.

SI.5. Damage quantification

Confocal set-up. Confocal images were taken with a customized Nikon AZ-100/C2+ confocal macroscope. The objective used was an AZ Plan Fluor 5x, with a focal length of 15 mm. The objective was upright and can zoom from 1x to 8x, with the use of 5x zoom for quantitative image analysis. Pixel size is 1.63 µm. Image size is 835 µm · 835 µm (512 px · 512 px).
We used an excitation wavelength $\lambda = 405$ nm and recorded emission from 450 nm to 550 nm.

Confocal image collection.

For systematic analysis, single optical sections were recorded in the area where the crack propagated. The images were taken perpendicular to the crack surface. Samples were immersed in glycerol to avoid refractive index mismatch at the crack surface (refractive index of PEA, PMA [5] and glycerol are respectively 1.464, 1.479 and 1.4722). The top of the sample was identified as the plane of maximal intensity. The focal plane was then displaced at 100 µm depth from the top of the sample for all quantifications. Laser and gain were adapted for each set of experiments.

Stable linear crack propagation occurred throughout most of our experiments. In this situation, two images at the beginning and end of the crack length were recorded for each side (four pictures per sample). In DA.DN. EA.EA networks, bifurcations appeared, leading to relatively large heterogeneities in local damage (see Fig. S9). To account for this heterogeneity, up to 10 images of the crack profile were recorded (5 image of the crack profile on each side). Damage values reported in the main text corresponds to mean and standard deviation on all images. In some materials (e.g. DA.TN. MA.MA samples), damage extends up to 1.5 mm from the crack surface, with a constant activation in the material (see Fig S8). In this case, several images were collected and stitched, in order to resolve the entire damage profile in the material.

Vignetting and flatfield correction. During imaging with the AZ-100/C2+ confocal macroscope, the low magnification of the optical system resulted in vignetting (inhomogeneous illumination and gradual intensity darkening toward the corners). To correct for vignetting, we measured the intensity $I_{\mathrm{FlatField}}$ in a calibration sample with homogeneous concentration of fluorescent calibration molecule. The corrected image of the crack surface I_{corr} was taken as $I_{\mathrm{corr}} = I_{\mathrm{original}} \,/\, I_{\mathrm{FlatField}}$. We furthermore restricted all quantitative analysis of damage to a distance of 500 µm along the crack profile for homogeneous crack profiles, and 650 µm for analysis on bifurcations (Fig. S9).

Calibration of fluorescence intensity. To convert fluorescence intensity to the concentration of activated molecules, we used calibration samples. The calibration molecule (9-phenylethynylanthracene) was mixed directly with linear PEA chains (Mw ~ 95,000 g.mol^{-1} in toluene from Sigma Aldrich). The solvent was evaporated under a hood for one day and under vacuum overnight, leading to calibration samples with a spatially homogenous concentration of fluorescent molecule. As fluorescence originates from the pi-extended anthracene group, which is present both in the calibration molecule and in the activated mechanophore and because the environment is the same (PEA chains), the calibration molecule is assumed to have the same fluorescence as the activated mechanophore. The concentration of activated mechanophore can thus be measured based on the intensity of the calibration molecule. By varying the concentration of the calibration molecule, a calibration curve of fluorescence intensity I vs activated mechanophore concentration c (mol.m^{-3}) was constructed, with $I \sim \alpha . c$.

Quantitative image analysis. To extract damage in the material, we measured the intensity profile $I(x)$ perpendicular to the crack edge and defined the background intensity I_{bkg} as the

residual intensity far from the crack (Fig. S8). The fraction of activated mechanophore $\phi(x)$ is calculated as $\phi(x) = \lambda_0^3 . \frac{\alpha}{c_0}(I(x) - I_{\text{bkg}})$ with $c_0^{\text{EA}} = 2.237$ mol.m^{-3}, $c_0^{\text{MA}} = 2.834$ mol.m^{-3}, α is the coefficient obtained from the calibration curve and λ_0 the prestretch.

The areal density of broken bonds is calculated as $\Sigma = 2\nu_x \int \phi(x)\mathrm{d}x$. For multiple networks, with $\lambda_0 > 1$, the density ν_x decreases with respect to initial density of cross-linker ν_x^0 in the single networks, as $\nu_x = 1/\lambda_0^3 . \nu_x^0$. The integrated damage can then be expressed as a sole function of ν_x^0, c_0 and α as $\Sigma = 2 . \nu_x^0 \int \frac{\alpha}{c_0}(I(x) - I_{\text{bkg}})\mathrm{d}x$.

Except for the TNDAMAMA samples (see below) Σ is calculated by integrating the damage up to ≈ 650 µm, a point at which the intensity reaches its background value.

Bulk activation in TN.DA.MA.MA samples.

While for most samples, the level of background intensity level of the fracture surfaces is in the same range, we observe for DA.TN. MA.MA samples a background intensity in the bulk reaching much larger values than for unactivated samples (Fig. S8). We attribute this background activation to failure of chains in the bulk of the material. As shown in Fig. S8, this bulk activation is controlled mostly by the strain at break (Fig. S8D). We define Σ in these samples by integrating the damage up to ≈ 1300 µm.

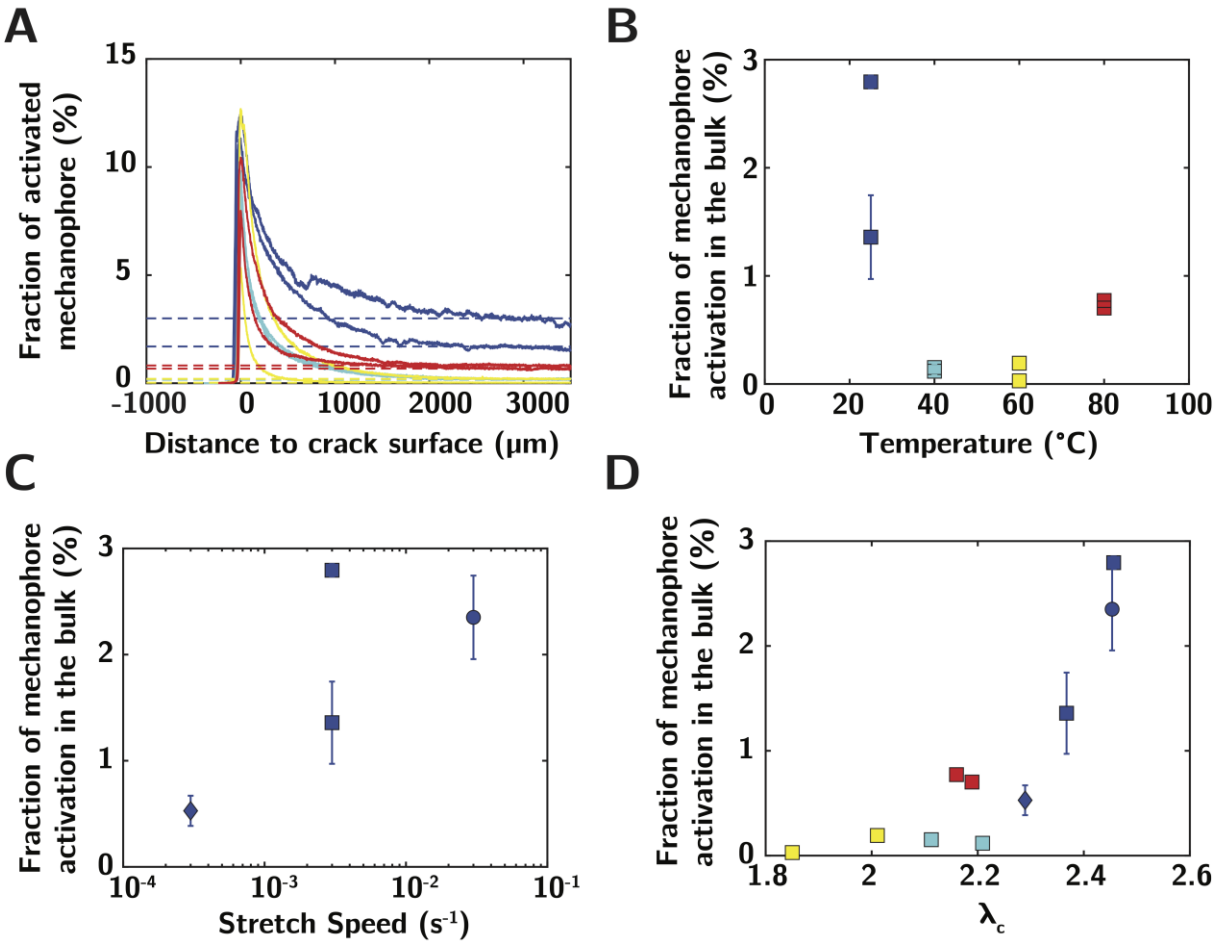

Fig S8. Bulk Activation in TN.MA.MA. **(A)** Fraction of activated mechanophore as a function of the distance to the crack surface. The dashed horizontal lines indicate the bulk level of activation. **(B-C)** Bulk activation of mechanophore as a function of (B) fracture temperature and (C) stretch speed. **(D)** Bulk activation of

mechanophore as a function of stretch at break λ_c. Blue, light blue, yellow and red points correspond to fracture performed respectively at 25, 40, 60 and 80 °C.

Analysis of bifurcations and inhomogeneous crack front in DA.DN.EA.EA.

In the case of DA.DN.EA.EA, crack bifurcation occurred during propagation. We can define in these conditions a value for the average damage per unit area of crack. As shown in Fig. S9, we measure the integrated intensity profile in the white dashed box (Figs. S9A-B), defined as the grey shaded region in Figs. S9C-D. This integrated damage is normalized by the unit area of crack (defined as the length of the red contour in Figs. S9A-B).

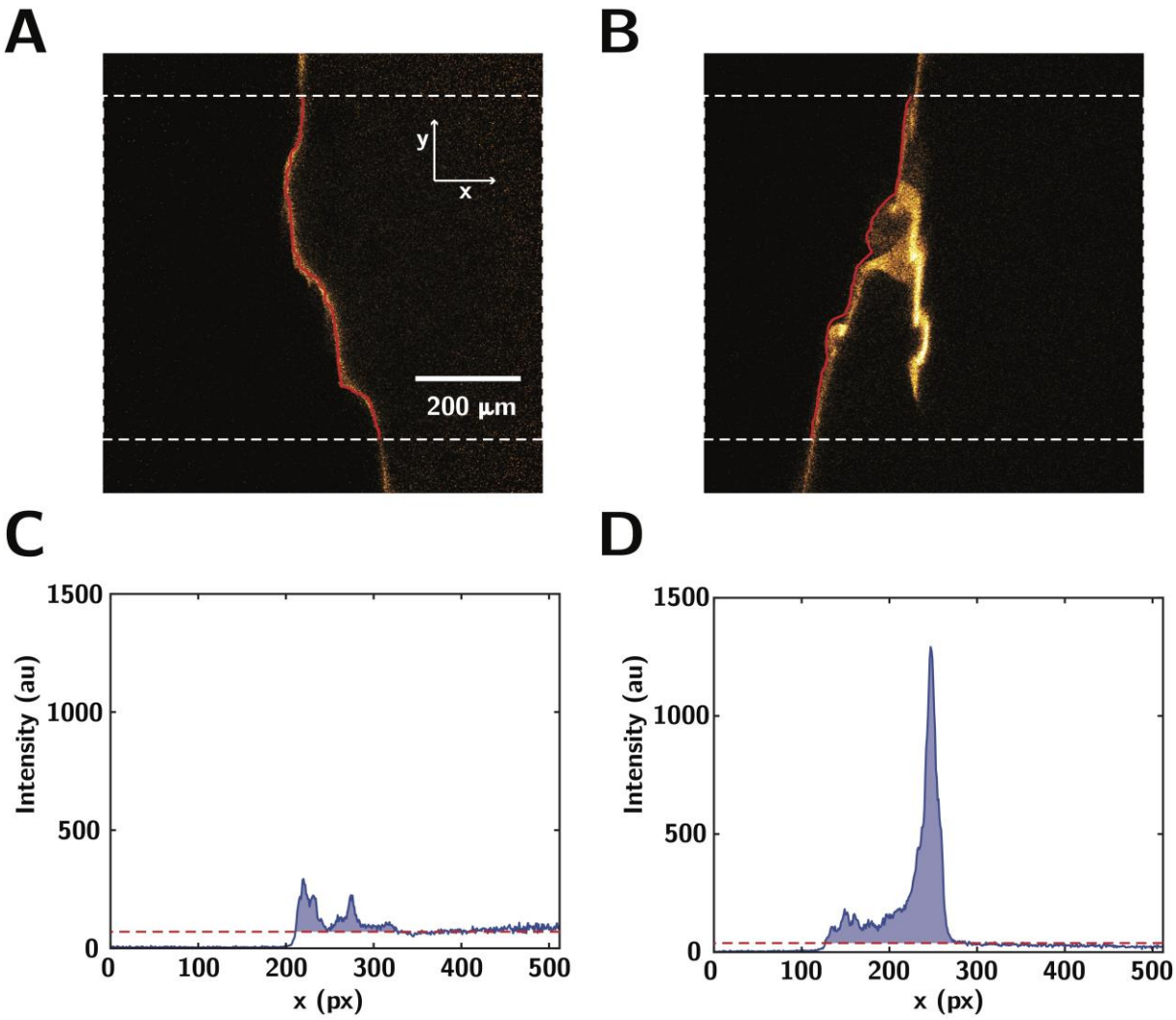

Fig S9. Bifurcation and inhomogeneous crack front in two DA.DN.EA.EA samples at 60°C. **(A, B)** Confocal map showing inhomogeneous crack profile. Red line shows crack contour. Dashed white box shows the region of interest for analysis. **(C, D)** Intensity profile, averaged over the *y* direction and plotted as a function of *x* (in units of pixel).

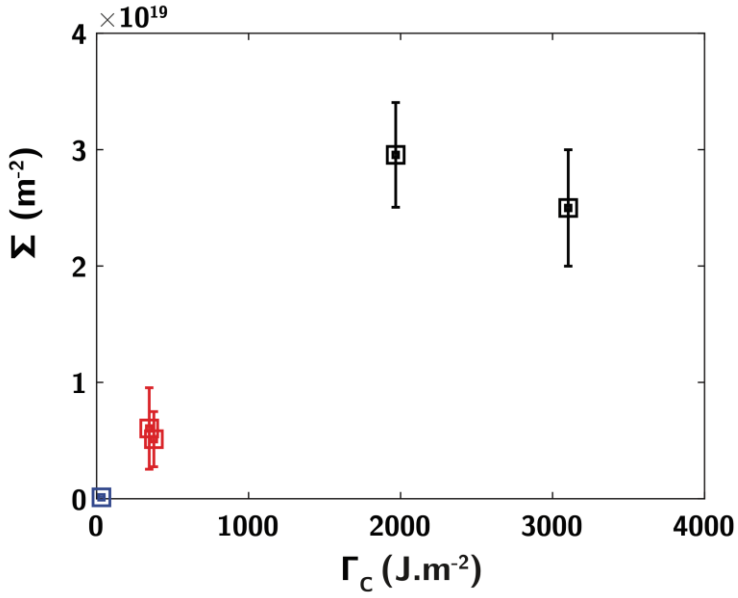

Fig. S10: Areal density of broken filler network chains as a function of fracture energy in threshold conditions for the three materials of the study. blue symbols (SN), red symbols (DN) and black symbols (TN).

Bibliography.

[1] P. Millereau *et al.*, "Mechanics of elastomeric molecular composites," *Proc. Natl. Acad. Sci. U. S. A.*, vol. 115, no. 37, pp. 9110–9115, 2018.

[2] J. Slootman *et al.*, "Quantifying rate- and temperature-dependent molecular damage in elastomer fracture," *Phys. Rev. X*, vol. 10, no. 4, p. 41045, 2020.

[3] E. Ducrot, Y. Chen, M. Bulters, R. P. Sijbesma, and C. Creton, "Toughening elastomers with sacrificial bonds and watching them break," *Science (80-.).*, vol. 344, no. 6180, pp. 186–189, 2014.

[4] H. W. Greensmith, "Rupture of rubber. X. The change in stored energy on making a small cut in a test piece held in simple extension," *J. Appl. Polym. Sci.*, vol. 7, no. 3, pp. 993–1002, 1963.

[5] J. E. Mark, "Polymer data handbook," *J. Am. Chem. Soc.*, vol. 131, no. 44, p. 1012, 1999.

[6] B. N. J. Persson and E. A. Brener, "Crack propagation in viscoelastic solids," *Phys. Rev. E - Stat. Nonlinear, Soft Matter Phys.*, vol. 71, no. 3, pp. 1–8, 2005.